

pubs.acs.org/macroletters Letter

# Chemical and Mechanical Tunability of 3D-Printed Dynamic Covalent Networks Based on Boronate Esters

Lindsay L. Robinson, Jeffrey L. Self, Alexander D. Fusi, Morgan W. Bates, Javier Read de Alaniz, Craig J. Hawker, Christopher M. Bates,\* and Caitlin S. Sample\*



Cite This: ACS Macro Lett. 2021, 10, 857–863



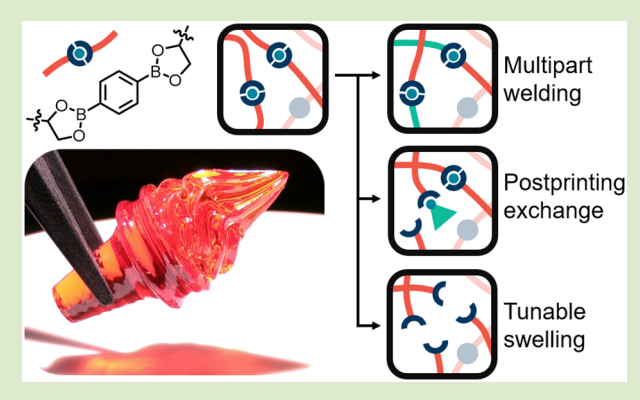
**ACCESS** 

III Metrics & More

Article Recommendations

Supporting Information

ABSTRACT: As the scope of additive manufacturing broadens, interest has developed in 3D-printed objects that are derived from recyclable resins with chemical and mechanical tunability. Dynamic covalent bonds have the potential to not only increase the sustainability of 3D-printed objects, but also serve as reactive sites for postprinting derivatization. In this study, we use boronate esters as a key building block for the development of catalyst-free, 3D-printing resins with the ability to undergo room-temperature exchange at the cross-linking sites. The orthogonality of boronate esters is exploited in fast-curing, oxygen-tolerant thiol—ene resins in which the dynamic character of 3D-printed objects can be modulated by the addition of a static, covalent cross-linker with no room-temperature bond exchange. This allows the mechanical properties of printed parts to be varied between those of a traditional thermoset and a vitrimer. Objects



printed with a hybrid dynamic/static resin exhibit a balance of structural stability (residual stress = 18%) and rapid exchange (characteristic relaxation time = 7 s), allowing for interfacial welding and postprinting functionalization. Modulation of the cross-linking density postprinting is enabled by selective hydrolysis of the boronate esters to generate networks with swelling capacities tunable from 1.3 to 3.3.

he ability of additive manufacturing (AM), also termed 3D printing, to produce objects with intricate, custom shapes has led to an increasing range of applications from biomedicine, 1-3 construction, 4 and energy 5 to aerospace. 6 In particular, vat photopolymerization printing techniques, such as stereolithography (SLA) and digital light processing (DLP), have enabled facile control over part complexity at the micron scale. While many early efforts focused on improving the resolution of printed objects, recent attention has been directed toward increasing the range of building blocks incorporated into additive manufacturing resin formulations (AM resins). This gives molecular-level control over network properties and functional group incorporation. For example, Lewis and co-workers have reported a method for 3D printing dielectric elastomer actuators that exhibit in-plane contractile actuation modes.<sup>8</sup> Similarly, Boydston and others have developed one-step, multimaterial strategies that allow for distinct mechanical properties to be spatially patterned within a 3D-printed object.

In addition to increasing the chemical complexity of AM resins, recent studies have focused on 3D-printed objects that can be modified postprinting. This work has evolved "4D printing" strategies, which generate objects that change shape in response to a stimulus. <sup>12,13</sup> Additionally, the inclusion of reactive chemical groups in the AM resin allows for surface

functionalities to be altered via postprinting modification, such as chromophore labeling or the growth of a polymer from tethered initiating sites.  $^{14-18}$ 

To enable even greater versatility over vat photopolymerization techniques, such as SLA and DLP, dynamic covalent bonds, whose exchangeable nature allows for the modification of both shape and chemical functionality, are an emerging area of significant potential. Dynamic bonds are used to great effect in extrusion-based processes such as fused filament fabrication (FFF)<sup>23,24</sup> and direct-ink writing (DIW),<sup>25–27</sup> demonstrating that reconfigurability serves the dual purpose of enhancing the performance of as-printed parts and allowing their transformation into new shapes during recycling. This is an important sustainability benefit considering the rapidly increasing quantity of 3D-printed material being produced every year. For vat systems, such as DLP, Ge and co-workers demonstrated the first 3D-printed reprocessable thermoset via

**Received:** April 20, 2021 **Accepted:** June 21, 2021 **Published:** June 23, 2021





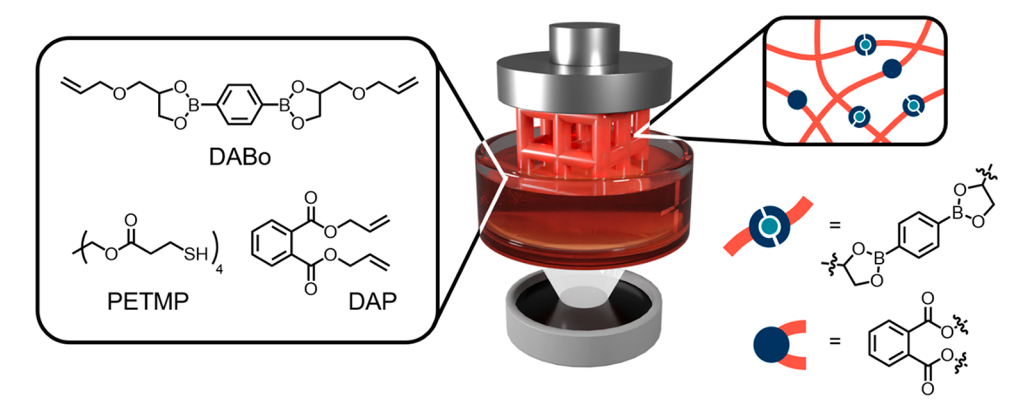


Figure 1. Overview of light-based 3D printing of resins, including dynamic boronate esters. Left: Monomers (diallyl boronate (DABo), pentaerithrytol tetrakis(3-mercaptopropionate) (PETMP), and diallyl phthalate (DAP)); Center: Graphical representation of the printer; Right: Schematic of the network structure containing a dynamic boronate ester and static diallyl phthalate cross-links.

the inclusion of hydroxyl and ester functionalities plus a zinc catalyst. The presence of catalyst and free hydroxyl groups enables the resulting objects to be remolded or repaired via transesterification.<sup>29–32</sup> Dynamic covalent bonds have also been employed in AM to weld 2D sheets into 3D parts through the exchange of hindered urea bonds.<sup>33</sup> While these reactions effectively allow for postprinting modification, they require high temperatures (>150 °C) to be activated, which may lead to thermal degradation or unwanted side reactions, particularly for sensitive functional groups. Interest has thus turned toward chemistries that are active at lower temperatures, including imines (120 °C),<sup>34</sup> Diels–Alder adducts (110 °C),<sup>35</sup> and disulfides (60–80 °C).<sup>36,37</sup>

In contrast with many other dynamic covalent chemistries (e.g., transesterification, <sup>19,38</sup> transcarbonation, <sup>39</sup> and urethane exchange <sup>40</sup>), boronate esters undergo catalyst-free transesterification with minimal heating (<60 °C), <sup>41–44</sup> in which partial hydrolysis facilitates exchange via a dissociative pathway. <sup>45,46</sup> The mild nature of boronate exchange has led to its use in the 3D printing of hydrogels via extrusion. <sup>47–52</sup> An additional feature of boronate esters is their stability during radical chemistry, <sup>42,45,46</sup> making them an appealing candidate for radical-based AM photopolymerization strategies.

This work presents a DLP-based approach toward the 3D printing of dynamic polymer networks containing boronate ester cross-linking units (Figure 1). Varying the relative incorporation of dynamic boronate and static phthalate cross-linkers in a photocurable thiol—ene resin yields control over the 3D-printing process and mechanical behavior of the resulting objects. The presence of a static cross-linker was found to be necessary for maintaining dimensional stability during printing, while the inclusion of dynamic bonds within the 3D-printed object allows for subsequent modification, both in structure and in function.

In the initial development of dynamic DLP resins, both acrylic- and thiol—ene-based systems were studied, with thiol—ene resins ultimately selected due to their oxygen tolerance, reduced shrinkage stress, and the ease of synthesizing a diallyl boronate monomer (DABo, Figure S1). This choice was further guided by pioneering studies from Sumerlin and coworkers, who demonstrated successful curing of thiol—ene networks containing structurally similar boronate esters. Additionally, recent studies demonstrate the effective translation of thiol—ene resins into SLA and DLP 3D-printing strategies. The potential disadvantages of thiol—ene

systems, namely, malodor and poor stability, were mitigated by the choice of a commonly used low-volatility thiol monomer (pentaerithrytol tetrakis(3-mercaptopropionate), PETMP) and the addition of small quantities of stabilizers (2,6-di-tert-butyl-4-methylphenol (BHT) as radical inhibitor and phenylphosphonic acid (PPA) as an acid costabilizer) to the resin mixture. With the addition of these stabilizers, which are analogous to those used previously with allyl-based monomers,  $^{60}$  the resin showed no notable change in viscosity over the course of printing (ca. 8 h) or while stored at  $-20\,^{\circ}\mathrm{C}$  (4+ weeks).

For bulk systems, a formulation containing stoichiometric quantities of DABo and PETMP, with phenylbis (2,4,6-trimethylbenzoyl)phosphine oxide (BAPO) as the initiator, cured rapidly (tack-free time < 1 min) when exposed to 405 nm light in an open-air benchtop mold. While this resin mixture yielded a highly cross-linked elastomer, initial attempts at 3D printing with an analogous formulation (Table S2) proved challenging, despite the curing kinetics remaining rapid, with a 100  $\mu$ m layer thickness achieved within 20 s (Figure S6). We concluded that the combination of rapid boronate ester exchange coupled with the elastomeric nature of the cured part ( $T_{\rm g} = -6$  °C, as measured by DSC, Figure S2) led to relaxation during printing, resulting in poor fidelity and eventual failure.

To increase dimensional stability, the dynamic nature of the diallyl boronate monomer was balanced by dilution with a static cross-linking monomer, that is, diallyl phthalate (DAP). Recent studies have shown that the introduction of static crosslinks into a dynamic covalent network can result in residual stresses upon relaxation that help maintain shape at the expense of the full recovery of mechanical properties upon reprocessing. 44,46,61,62 To investigate the effect of a static crosslinker, benchtop samples were prepared containing varying amounts of DABo and DAP (keeping the total allyl content constant), and the stress relaxation behavior was examined after curing (Figure S3). While the fully static sample (0 mol % DABo) showed minimal stress relaxation as expected for a highly cross-linked thermoset, the addition of a boronate monomer resulted in increasing relaxation. This data was further explored by fitting to a stretched exponential decay (Table S1), which allowed the identification of two regimes. As with previous hybrid static/dynamic systems, 44,61,62 samples with high percentages of dynamic monomer (60-100 mol % DABo) exhibited the full stress relaxation characteristic of

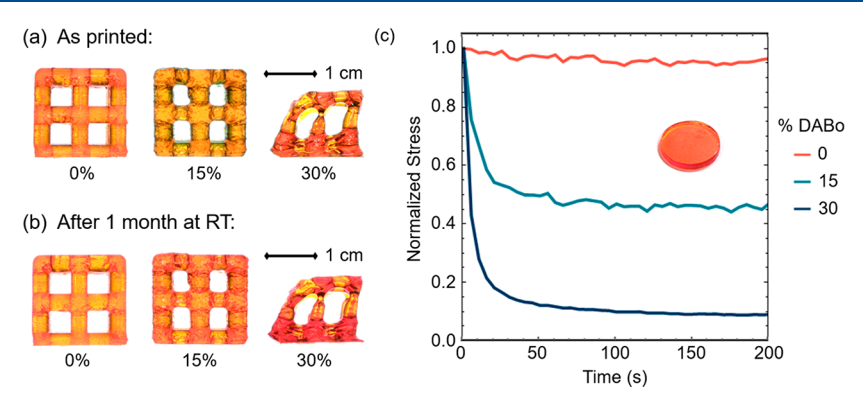


Figure 2. Images of 3D printed cubic lattices with 0, 15, and 30 mol % DABo incorporation. (a) As printed and (b) after one month at room temperature. (c) Room-temperature stress relaxation of 3D printed cylindrical samples, 0, 15, and 30 mol % DABo incorporation, measured in shear via parallel-plate (8 mm) rheometry with a strain of 0.1%. Inset shows an image of a representative cylindrical sample.

traditional covalent adaptable networks, with little difference in characteristic relaxation times among formulations containing 60 or 100 mol % DABo. However, below a critical threshold of DABo monomer loading, a percolating nondynamic network is formed, resulting in an increase in the characteristic relaxation time (from 23 s for 60 mol % DABo to 56 s for 40 mol % DABo). Additionally, the retention of residual stress (6% for 40 mol % DABo, increasing to 24% for 20 mol % DABo) was observed. Notably, this transition occurs at a lower dynamic loading than that predicted by theory (≈67% for a tetrafunctional cross-linker),61 which is consistent with empirical observations for similar systems.<sup>44,46</sup> This discrepancy can be attributed to the structural imperfections inevitably present within an experimental network, including incomplete conversion, loop formation, and dangling chains, which are not accounted for by theory. 63 These imperfections are expected to arise at least in part from minor hydrolysis of the boronate cross-links, which has been observed under ambient conditions.46

From these benchtop, bulk-cured results, it was apparent that low DABo loadings (<40 mol %) led to a desirable balance of rapid relaxation and reinforcing residual stress. To investigate how these mixed static/dynamic systems behave during 3D printing, resins with DABo incorporations from 0-30 mol % were prepared (Table S3), and a cubic lattice was printed using a DLP system (Figure 2a). The effect of varied dynamic character is evident, as both the fully static (0 mol % DABo) and 15 mol % DABo samples printed successfully, while the 30 mol % DABo showed failure during the print as well as creep immediately afterward. This relaxation in the 30 mol % DABo system can again be attributed in large part to the rapidity of boronate exchange at room temperature as well as the low  $T_{\rm g}$  (18 °C) of the thiol-ene network (measured by DMA, Figure S11). However, we note that the low conversions achieved during the printing process also appear to play a role. Upon the completion of a standard postprint photochemical cure, the 3D-printed objects achieved high conversions, as observed by the substantial reduction in thiol signal (FTIR, Figure S7) and allyl resonances (solid-state NMR, Figure S8) and large gel fractions (>90%, Table S4). No visible creep was observed for prolonged periods at room temperature, even in the case of samples with 30 mol % DABo (Figure 2b).

To further study the interplay of dynamic and static crosslinking, cylindrical samples with 0, 15, and 30 mol % DABo incorporation were printed, and room-temperature stress relaxation measurements were performed. The printed samples exhibited similar behavior when compared to benchtop, bulk-cured samples, with decreasing residual stress arising from increased incorporation of DABo. The measurements of the printed samples show that the 30 mol % DABo system retains less than 10% of the applied stress, which, as is evident from the visual results, is insufficient to reinforce the network. As a result, the window of resin formulations for successful printing was identified as <30 mol % DABo.

By decreasing the loading of dynamic DABo cross-linker to 25 mol %, a range of high complexity 3D lattices were printed with excellent fidelity (Figure 3). All three contain well-defined

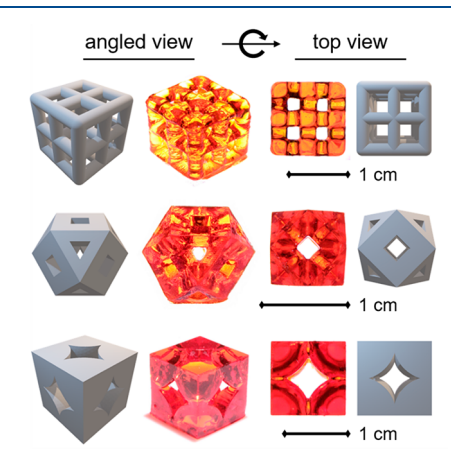
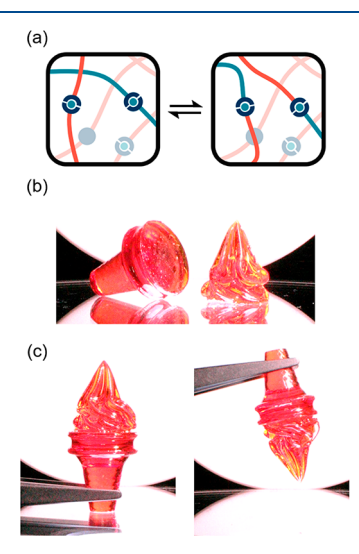


Figure 3. 3D models of three different lattices (left and right) and side-/top-down images of the resulting 3D-printed objects (center) from a resin containing 25 mol % DABo. Scale bars represent 1 cm.

internal structures that were preserved in the final object, with the sharpness of corners and edges not softened by midprint creep. Furthermore, despite the 1:3 molar ratio of dynamic (DABo) versus static (DAP) cross-linker, cylindrical samples printed with 25 mol % DABo incorporation revealed rapid stress relaxation with a residual stress of less than 20% (Figure S12). In addition, the room-temperature relaxation results in the noticeable smoothing of layer boundaries and surface defects relative to objects printed with the 0 mol % DABo formulation (Figure S13). This apparent reduction in interfacial boundaries highlights the potential of using low loadings of a room-temperature-exchangeable cross-link to achieve 3D-printed objects with in situ smoothing of the layered structures inherent to DLP and SLA techniques.

A key feature of dynamic boronate ester cross-linking is the room-temperature, catalyst-free exchange between functional groups within the network (Figure 4a), which enables



**Figure 4.** (a) Graphical representation of dynamic exchange between network strands involving boronate cross-link units. Images of (b) ice cream cone and ice cream as printed and (c) welded after 16 h at 65 °C.

postprinting modification such as interfacial welding and secondary functionalization. While the presence of a static DAP cross-linker prevents fully cohesive self-healing, the boronate ester loading is sufficient to permit cross-linking between parts after heating to 65 °C (Figure S14). To demonstrate how this cross-linking allows multipart welding, a model ice cream cone and ice cream were printed separately (Figure 4b). Upon contact between the two parts and a thermal treatment, boronate esters exchanged across the interface. The resultant ensemble was able to support its own weight upon inversion (Figure 4c and Supporting Information, video), while no welding was observed for the corresponding 0 mol % DABo sample subjected to the same conditions (Figure S15 and Supporting Information, video).

In addition to multipart welding, the presence of dynamic covalent bonds also allows for molecular-level tunability via boronate ester exchange. For example, treating DABocontaining networks with a boronic acid, in this case, 3-(dansylamino)phenylboronic acid (DAPBA), results in a fraction of the cross-links being replaced by the DAPBA fluorophore, as shown in Figure 5a. To illustrate the orthogonal nature of this functionalization process, printed samples containing either 0 mol % or 25 mol % DABo were placed in a solution of DAPBA at room temperature, followed by Soxhlet extraction to remove noncovalently bound fluorophore. The presence of the fluorophore in each network was then monitored spectroscopically via fluorimetry. Interestingly, a notably more intense DAPBA emission peak was observed for the dynamic network containing 25 mol % of DABo units compared to the fully static network containing 0 mol % DABo. This difference in emission intensity is rationalized by the ability of the boronate esters to undergo transesterification with diols, leading to the covalent attachment of fluorophore within the DABo-containing networks (Figure 5b). This transesterification of the DABo cross-linking sites can also be used to selectively functionalize 3D-printed

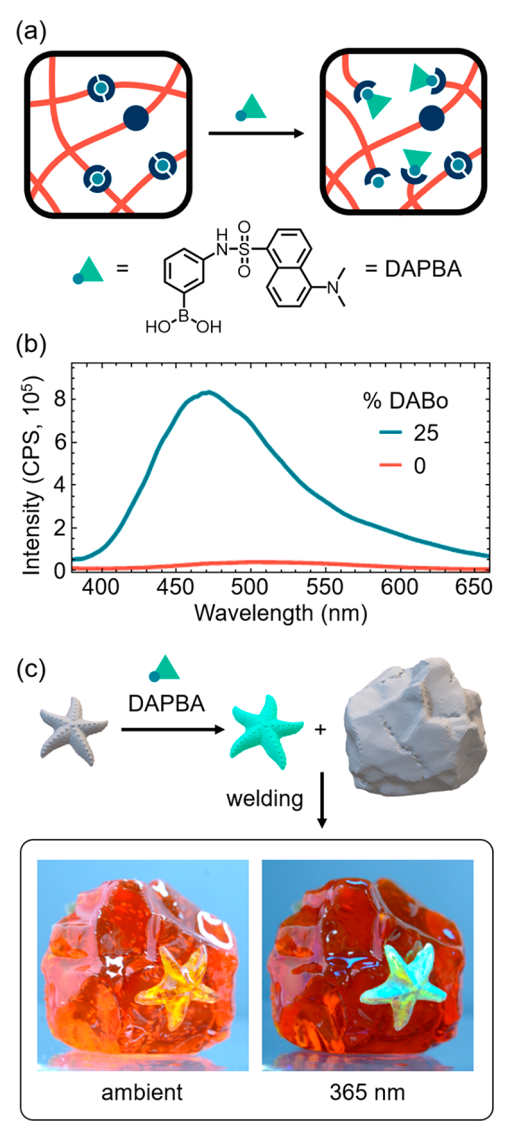
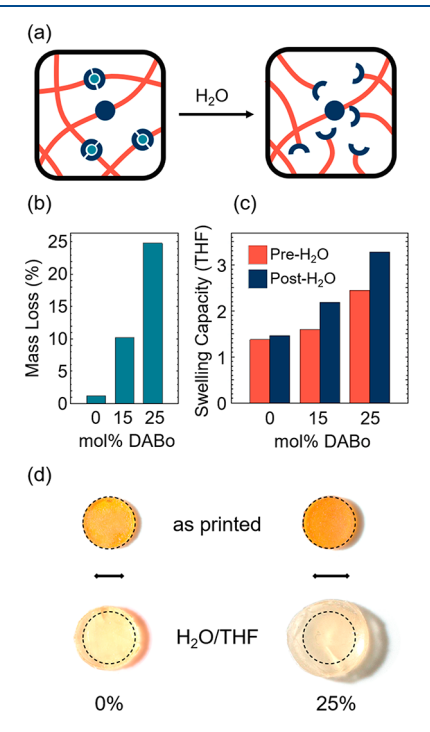


Figure 5. (a) Graphical representation of the exchange reaction between network boronate esters and a fluorescent boronic acid (3-(dansylamino)phenylboronic acid (DAPBA). (b) Fluorimetry results after exchange and Soxhlet extraction for the 25 mol % DABo sample and a 0 mol % DABo control. (c) Demonstration of dynamic exchange with DAPBA in a printed starfish sample that was subsequently welded to a printed rock, yielding a mixed fluorescent/nonfluorescent system that was imaged under both ambient light and with irradiation from a 365 nm lamp.

objects by either partial swelling with DAPBA solution, leading to exchange only in the areas exposed to the boronic acid (Figure S19) or through a combined functionalization/welding approach (Figure 5c). The latter involves the printing of two separate objects, of which only one is exposed to the DAPBA solution, and then both objects are welded together to form the final structure. Using this convergent approach, a 3D-printed starfish (25 mol % DABo) was exposed to the fluorophore solution and then subsequently welded to a 3D-printed rock (25 mol % DABo) that had not been exposed to DAPBA. This resulted in a hybrid fluorescent/nonfluorescent system, illustrating the power of this modular strategy for fabricating spatially functionalized 3D printed ensembles.

The versatility of boronate esters as a modular cross-linking unit can be further examined based on their ability to undergo

facile hydrolysis in the presence of water. The consequence of this process for a dual network containing both labile and static cross-links is that hydrolysis of the boronate esters leads to a programmable decrease in cross-linking density, while the stability of the static DAP-derived cross-links prevents full dissolution (Figure 6a). Cylindrical samples were printed



**Figure 6.** (a) Cartoon of boronate ester hydrolysis. (b) Decrease in dry sample mass after exposure to 10% (v/v)  $H_2O$  in THF. (c) THF swelling capacity for samples containing varied quantities of DABo before (red) and after (blue) exposure to 10% (v/v)  $H_2O$  in THF. (d) Demonstration of difference in swelling between 0 mol % and 25 mol % DABo samples, both exposed to 10% (v/v)  $H_2O$  in THF.

containing DABo loadings of 0, 15, and 25 mol % and subsequently exposed to a solution of 10% (v/v) H<sub>2</sub>O in THF. The dry masses of the samples were measured before and after this exposure, with the larger mass loss observed for samples with higher DABo loadings, which is suggestive of the hydrolytic cleavage of the boronate esters (Figure 6b). This hydrolysis is further supported by the changes in swelling capacity (defined as  $(m_2 - m_1)/m_1$ , where  $m_1$  is the dry mass and  $m_2$  is the solvated mass) of the samples, as measured in THF before and after exposure to water (Figure 6c). While the larger swelling capacity of the samples with more DABo crosslinker can be attributed in part to polarity differences, as an upward trend is apparent in the prehydrolyzed samples, this increase is magnified postexposure to water. Notably, after exposure to water, the 25 mol % DABo sample exhibits more than double the swelling capacity of the 0 mol % analogue. This additional swelling capacity is attributed to a combination of decreased cross-linking density and changing polarity arising from the liberation of diols upon hydrolysis of the boronate esters. The resulting difference in swelling behavior is visually apparent, with the 25 mol % sample increasing in size to a much larger degree than the 0 mol % control sample (Figure

In conclusion, we demonstrated a DLP-based strategy for the 3D-printing of dynamic covalent networks based on boronate esters. The degree of relaxation in printed parts can be tuned via the relative percentage of dynamic boronate esters versus static phthalate cross-links, with the critical boronate concentration (relative to total allyl monomer content) found to be 25 mol %. Using resins containing up to 25 mol % DABo, objects were fabricated with complex three-dimensional geometries that exhibit dynamic character, which allows for the welding of multiple objects. Furthermore, exchange with free boronic acids enables the postfabrication introduction of chemical motifs, such as the spatial patterning of fluorescent groups. Selective hydrolysis of the boronate esters is also possible, which gives solvated networks with a degree of swelling dependent on the initial loading of dynamic DABo cross-linker. As a result, the inclusion of exchangeable boronate cross-links in a thiol-ene resin is a powerful strategy for the production of 3D-printed dynamic thermosets that can be modified under mild conditions. Future work will broaden the scope of this approach, including the investigation of higher- $T_{\sigma}$ monomers for increased dimensional stability during printing and the design of hydrophilic systems for fabricating biocompatible, dynamic 3D hydrogels.

### ASSOCIATED CONTENT

## Supporting Information

The Supporting Information is available free of charge at https://pubs.acs.org/doi/10.1021/acsmacrolett.1c00257.

Experimental details and supporting figures and tables (PDF)

Welding demonstration (MP4)

# AUTHOR INFORMATION

# **Corresponding Authors**

Caitlin S. Sample — Materials Department, University of California, Santa Barbara, California 93106, United States; Present Address: Department of Chemistry, University of Minnesota, Twin Cities, Minneapolis, MN 55408, United States; Email: sampl128@umn.edu

Christopher M. Bates — Department of Chemistry and Biochemistry, Materials Research Laboratory, Materials Department, and Department of Chemical Engineering, University of California, Santa Barbara, California 93106, United States; Occid.org/0000-0002-1598-794X; Email: cbates@ucsb.edu

# **Authors**

Lindsay L. Robinson – Department of Chemistry and Biochemistry, University of California, Santa Barbara, California 93106, United States

Jeffrey L. Self – Department of Chemistry and Biochemistry, University of California, Santa Barbara, California 93106, United States

Alexander D. Fusi – Materials Research Laboratory, University of California, Santa Barbara, California 93106, United States

Morgan W. Bates — California NanoSystems Institute, University of California, Santa Barbara, California 93106, United States; © orcid.org/0000-0002-8939-2682

Javier Read de Alaniz – Department of Chemistry and Biochemistry and California NanoSystems Institute, University of California, Santa Barbara, California 93106, United States; orcid.org/0000-0003-2770-9477

Craig J. Hawker — Department of Chemistry and Biochemistry, Materials Research Laboratory, Materials Department, and California NanoSystems Institute, University of California, Santa Barbara, California 93106, United States; orcid.org/0000-0001-9951-851X

Complete contact information is available at: https://pubs.acs.org/10.1021/acsmacrolett.1c00257

#### **Author Contributions**

All authors have given approval to the final version of the manuscript.

#### **Notes**

The authors declare no competing financial interest.

#### ACKNOWLEDGMENTS

The research was sponsored by the U.S. Army Research Office and was accomplished under Contract Number W911NF-09-D-0001 and Cooperative Agreement W911NF-19-2-0026 for the Institute for Collaborative Biotechnologies. This work was supported by the BioPACIFIC Materials Innovation Platform of the National Science Foundation under Award No. DMR-1933487. The research reported here made use of shared facilities of the UCSB MRSEC (NSF DMR 1720256), a member of the Materials Research Facilities Network (www. mrfn.org). This work was supported in part by NSF Major Research Instrumentation award, MRI-1920299, for magnetic resonance instrumentation. Facility support by the California Nanosystems Institute is also gratefully acknowledged. The views and conclusions contained in this document are those of the authors and should not be interpreted as representing the official policies, either expressed or implied, of the U.S. Government. The U.S. Government is authorized to reproduce and distribute reprints for Government purposes notwithstanding any copyright notation herein. L.L.R., C.S.S., and J.L.S. are thankful for support by National Science Foundation Graduate Research Fellowships. The authors would like to thank Dave Bothman for his engineering insight, Dr. Amanda Strom and Dr. Rachel Behrens for their help with characterization, and Friedrich Stricker and Dr. Soyoung E. Seo for their imaging assistance. We would also like to thank Dr. Neil D. Dolinski, Dr. Soyoung E. Seo, and Dr. Zhishuai Geng for their helpful discussions regarding 3D-printing and organic synthesis. Additionally, we would like to thank Dr. Jerry Hu for collecting and analyzing the solid-state NMR data.

## REFERENCES

- (1) Murphy, S. V.; Atala, A. 3D Bioprinting of Tissues and Organs. *Nat. Biotechnol.* **2014**, *32*, 773–785.
- (2) Zhu, W.; Ma, X.; Gou, M.; Mei, D.; Zhang, K.; Chen, S. 3D Printing of Functional Biomaterials for Tissue Engineering. *Curr. Opin. Biotechnol.* **2016**, *40*, 103–112.
- (3) Yan, Q.; Dong, H.; Su, J.; Han, J.; Song, B.; Wei, Q.; Shi, Y. A Review of 3D Printing Technology for Medical Applications. *Engineering* **2018**, *4*, 729–742.
- (4) Tay, Y. W. D.; Panda, B.; Paul, S. C.; Noor Mohamed, N. A.; Tan, M. J.; Leong, K. F. 3D Printing Trends in Building and Construction Industry: A Review. *Virtual Phys. Prototyp.* **2017**, *12*, 261–276.
- (5) Browne, M. P.; Redondo, E.; Pumera, M. 3D Printing for Electrochemical Energy Applications. *Chem. Rev.* **2020**, *120*, 2783–2810.
- (6) Joshi, S. C.; Sheikh, A. A. 3D Printing in Aerospace and Its Long-Term Sustainability. Virtual Phys. Prototyp. 2015, 10, 175–185.

- (7) Narupai, B.; Nelson, A. 100th Anniversary of Macromolecular Science Viewpoint: Macromolecular Materials for Additive Manufacturing. ACS Macro Lett. 2020, 9, 627–638.
- (8) Chortos, A.; Hajiesmaili, E.; Morales, J.; Clarke, D. R.; Lewis, J. A. 3D Printing of Interdigitated Dielectric Elastomer Actuators. *Adv. Funct. Mater.* **2020**, *30*, 1907375.
- (9) Dolinski, N. D.; Page, Z. A.; Callaway, E. B.; Eisenreich, F.; Garcia, R. V.; Chavez, R.; Bothman, D. P.; Hecht, S.; Zok, F. W.; Hawker, C. J. Solution Mask Liquid Lithography (SMaLL) for One-Step, Multimaterial 3D Printing. *Adv. Mater.* **2018**, *30*, 1800364.
- (10) Schwartz, J. J.; Boydston, A. J. Multimaterial Actinic Spatial Control 3D and 4D Printing. *Nat. Commun.* **2019**, *10*, 791.
- (11) Dolinski, N. D.; Callaway, E. B.; Sample, C. S.; Gockowski, L. F.; Chavez, R.; Page, Z. A.; Eisenreich, F.; Hecht, S.; Valentine, M. T.; Zok, F. W.; Hawker, C. J. Tough Multimaterial Interfaces through Wavelength-Selective 3D Printing. ACS Appl. Mater. Interfaces 2021, 13, 22065–22072.
- (12) Sydney Gladman, A.; Matsumoto, E. A.; Nuzzo, R. G.; Mahadevan, L.; Lewis, J. A. Biomimetic 4D Printing. *Nat. Mater.* **2016**, *15*, 413–418.
- (13) Kuang, X.; Roach, D. J.; Wu, J.; Hamel, C. M.; Ding, Z.; Wang, T.; Dunn, M. L.; Qi, H. J. Advances in 4D Printing: Materials and Applications. *Adv. Funct. Mater.* **2019**, *29*, 1805290.
- (14) Guo, Q.; Cai, X.; Wang, X.; Yang, J. Paintable" 3D Printed Structures via a Post-ATRP Process with Antimicrobial Function for Biomedical Applications. *J. Mater. Chem. B* **2013**, *1*, 6644–6649.
- (15) Wang, X.; Cai, X.; Guo, Q.; Zhang, T.; Kobe, B.; Yang, J. I3DP, a Robust 3D Printing Approach Enabling Genetic Post-Printing Surface Modification. *Chem. Commun.* **2013**, *49*, 10064–10066.
- (16) Zhang, Z.; Corrigan, N.; Bagheri, A.; Jin, J.; Boyer, C. A Versatile 3D and 4D Printing System through Photocontrolled RAFT Polymerization. *Angew. Chem.* **2019**, *131*, 18122–18131.
- (17) Bagheri, A.; Engel, K. E.; Bainbridge, C. W. A.; Xu, J.; Boyer, C.; Jin, J. 3D Printing of Polymeric Materials Based on Photo-RAFT Polymerization. *Polym. Chem.* **2020**, *11*, 641–647.
- (18) Bagheri, A.; Bainbridge, C. W. A.; Engel, K. E.; Qiao, G. G.; Xu, J.; Boyer, C.; Jin, J. Oxygen Tolerant PET-RAFT Facilitated 3D Printing of Polymeric Materials under Visible LEDs. ACS Appl. Polym. Mater. 2020, 2, 782–790.
- (19) Montarnal, D.; Capelot, M.; Tournilhac, F.; Leibler, L. Silicalike Malleable Materials from Permanent Organic Networks. *Science* **2011**, 334, 965–968.
- (20) Kloxin, C. J.; Bowman, C. N. Covalent Adaptable Networks: Smart, Reconfigurable and Responsive Network Systems. *Chem. Soc. Rev.* **2013**, *42*, 7161–7173.
- (21) Denissen, W.; Winne, J. M.; Du Prez, F. E. Vitrimers: Permanent Organic Networks with Glass-like Fluidity. *Chem. Sci.* **2016**, *7*, 30–38.
- (22) Zou, W.; Dong, J.; Luo, Y.; Zhao, Q.; Xie, T. Dynamic Covalent Polymer Networks: From Old Chemistry to Modern Day Innovations. *Adv. Mater.* **2017**, *29*, 1606100.
- (23) Davidson, J. R.; Appuhamillage, G. A.; Thompson, C. M.; Voit, W.; Smaldone, R. A. Design Paradigm Utilizing Reversible Diels-Alder Reactions to Enhance the Mechanical Properties of 3D Printed Materials. ACS Appl. Mater. Interfaces 2016, 8, 16961–16966.
- (24) Yang, K.; Grant, J. C.; Lamey, P.; Joshi-Imre, A.; Lund, B. R.; Smaldone, R. A.; Voit, W. Diels—Alder Reversible Thermoset 3D Printing: Isotropic Thermoset Polymers via Fused Filament Fabrication. *Adv. Funct. Mater.* **2017**, 27, 1700318.
- (25) Shi, Q.; Yu, K.; Kuang, X.; Mu, X.; Dunn, C. K.; Dunn, M. L.; Wang, T.; Jerry Qi, H. Recyclable 3D Printing of Vitrimer Epoxy. *Mater. Horiz.* **2017**, *4*, 598–607.
- (26) Davidson, E. C.; Kotikian, A.; Li, S.; Aizenberg, J.; Lewis, J. A. 3D Printable and Reconfigurable Liquid Crystal Elastomers with Light-Induced Shape Memory via Dynamic Bond Exchange. *Adv. Mater.* **2020**, 32, 1905682.
- (27) Zheng, M.; Guo, Q.; Yin, X.; Getangama, N. N.; de Bruyn, J.; Xiao, J.; Bai, Y.; Liu, M.; Yang, J. Direct Ink Writing of Recyclable and

- In-Situ Repairable Photothermal Polyurethane for Sustainable 3D Printing Development. *J. Mater. Chem. A* **2021**, *9*, 6981.
- (28) Voet, V. S. D.; Guit, J.; Loos, K. Sustainable Photopolymers in 3D Printing: A Review on Biobased, Biodegradable, and Recyclable Alternatives. *Macromol. Rapid Commun.* **2021**, 42, 2000475.
- (29) Zhang, B.; Kowsari, K.; Serjouei, A.; Dunn, M. L.; Ge, Q. Reprocessable Thermosets for Sustainable Three-Dimensional Printing. *Nat. Commun.* **2018**, *9*, 1831.
- (30) Chen, Z.; Yang, M.; Ji, M.; Kuang, X.; Qi, H. J.; Wang, T. Recyclable Thermosetting Polymers for Digital Light Processing 3D Printing. *Mater. Des.* **2021**, *197*, 109189.
- (31) Rossegger, E.; Höller, R.; Reisinger, D.; Strasser, J.; Fleisch, M.; Griesser, T.; Schlögl, S. Digital Light Processing 3D Printing with Thiol–Acrylate Vitrimers. *Polym. Chem.* **2021**, *12*, 639–644.
- (32) Rossegger, E.; Moazzen, K.; Fleisch, M.; Schlogl, S. Locally Controlling Dynamic Exchange Reactions in 3D Printed Thiol-Acrylate Vitrimers Using Dual-Wavelength Digital Light Processing. *Polym. Chem.* **2021**, *12*, 3077–3083.
- (33) Fang, Z.; Song, H.; Zhang, Y.; Jin, B.; Wu, J.; Zhao, Q.; Xie, T. Modular 4D Printing via Interfacial Welding of Digital Light-Controllable Dynamic Covalent Polymer Networks. *Matter* **2020**, 2 (5), 1187–1197.
- (34) Miao, J. T.; Ge, M.; Peng, S.; Zhong, J.; Li, Y.; Weng, Z.; Wu, L.; Zheng, L. Dynamic Imine Bond-Based Shape Memory Polymers with Permanent Shape Reconfigurability for 4D Printing. ACS Appl. Mater. Interfaces 2019, 11 (43), 40642–40651.
- (35) Durand-Silva, A.; Cortes-Guzman, K. P.; Johnson, R. M.; Perera, S. D.; Diwakara, S. D.; Smaldone, R. A. Balancing Self-Healing and Shape Stability in Dynamic Covalent Photoresins for Stereolithography 3D Printing. ACS Macro Lett. 2021, 10, 486–491.
- (36) Yu, K.; Xin, A.; Du, H.; Li, Y.; Wang, Q. Additive Manufacturing of Self-Healing Elastomers. NPG Asia Mater. 2019, 11. 7.
- (37) Li, X.; Yu, R.; He, Y.; Zhang, Y.; Yang, X.; Zhao, X.; Huang, W. Self-Healing Polyurethane Elastomers Based on a Disulfide Bond by Digital Light Processing 3D Printing. *ACS Macro Lett.* **2019**, *8*, 1511–1516.
- (38) Self, J. L.; Sample, C. S.; Levi, A. E.; Li, K.; Xie, R.; Read de Alaniz, J.; Bates, C. M. Dynamic Bottlebrush Polymer Networks: Self-Healing in Super-Soft Materials. *J. Am. Chem. Soc.* **2020**, *142*, 7567–7573.
- (39) Snyder, R. L.; Fortman, D. J.; De Hoe, G. X.; Hillmyer, M. A.; Dichtel, W. R. Reprocessable Acid-Degradable Polycarbonate Vitrimers. *Macromolecules* **2018**, *51* (2), 389–397.
- (40) Denissen, W.; Rivero, G.; Nicolay, R.; Leibler, L.; Winne, J. M.; Du Prez, F. E. Vinylogous Urethane Vitrimers. *Adv. Funct. Mater.* **2015**, 25, 2451–2457.
- (41) Cromwell, O. R.; Chung, J.; Guan, Z. Malleable and Self-Healing Covalent Polymer Networks through Tunable Dynamic Boronic Ester Bonds. *J. Am. Chem. Soc.* **2015**, *137*, 6492–6495.
- (42) Röttger, M.; Domenech, T.; van der Weegen, R.; Breuillac, A.; Nicolaÿ, R.; Leibler, L. High-Performance Vitrimers from Commodity Thermoplastics through Dioxaborolane Metathesis. *Science* **2017**, 356, 62–65.
- (43) Breuillac, A.; Kassalias, A.; Nicolaÿ, R. Polybutadiene Vitrimers Based on Dioxaborolane Chemistry and Dual Networks with Static and Dynamic Cross-Links. *Macromolecules* **2019**, *52* (18), 7102–7113.
- (44) Meng, F.; Saed, M. O.; Terentjev, E. M. Elasticity and Relaxation in Full and Partial Vitrimer Networks. *Macromolecules* **2019**, 52 (19), 7423–7429.
- (45) Cash, J. J.; Kubo, T.; Bapat, A. P.; Sumerlin, B. S. Room-Temperature Self-Healing Polymers Based on Dynamic-Covalent Boronic Esters. *Macromolecules* **2015**, *48*, 2098–2106.
- (46) Cash, J. J.; Kubo, T.; Dobbins, D. J.; Sumerlin, B. S. Maximizing the Symbiosis of Static and Dynamic Bonds in Self-Healing Boronic Ester Networks. *Polym. Chem.* **2018**, *9* (15), 2011–2020.
- (47) Wang, Y.; Yu, H.; Yang, H.; Hao, X.; Tang, Q.; Zhang, X. An Injectable Interpenetrating Polymer Network Hydrogel with Tunable

- Mechanical Properties and Self-Healing Abilities. *Macromol. Chem. Phys.* **2017**, 218, 1700348.
- (48) Biswas, A.; Maiti, S.; Kalaskar, D. M.; Das, A. K. Redox-Active Dynamic Self-Supporting Thixotropic 3D-Printable G-Quadruplex Hydrogels. *Chem. Asian J.* **2018**, *13*, 3928–3934.
- (49) Biswas, A.; Malferrari, S.; Kalaskar, D. M.; Das, A. K. Arylboronate Esters Mediated Self-Healable and Biocompatible Dynamic G-Quadruplex Hydrogels as Promising 3D-Bioinks. *Chem. Commun.* **2018**, *54*, 1778–1781.
- (50) Huang, W.; Qi, C.; Gao, Y. Injectable Self-Healable Nanocomposite Hydrogels with Mussel-Inspired Adhesive Properties for 3D Printing Ink. ACS Appl. Nano Mater. 2019, 2, 5000–5008.
- (51) Shi, W.; Hass, B.; Kuss, M. A.; Zhang, H.; Ryu, S.; Zhang, D.; Li, T.; Li, Y.-l.; Duan, B. Fabrication of Versatile Dynamic Hyaluronic Acid-Based Hydrogels. *Carbohydr. Polym.* **2020**, 233, 115803.
- (52) Ghosh, T.; Biswas, A.; Gavel, P. K.; Das, A. K. Engineered Dynamic Boronate Ester-Mediated Self-Healable Biocompatible G-Quadruplex Hydrogels for Sustained Release of Vitamins. *Langmuir* **2020**, *36*, 1574–1584.
- (53) Barker, I. A.; Ablett, M. P.; Gilbert, H. T. J.; Leigh, S. J.; Covington, J. A.; Hoyland, J. A.; Richardson, S. M.; Dove, A. P. A Microstereolithography Resin Based on Thiol-Ene Chemistry: Towards Biocompatible 3D Extracellular Constructs for Tissue Engineering. *Biomater. Sci.* **2014**, *2*, 472–475.
- (54) Oesterreicher, A.; Wiener, J.; Roth, M.; Moser, A.; Gmeiner, R.; Edler, M.; Pinter, G.; Griesser, T. Tough and Degradable Photopolymers Derived from Alkyne Monomers for 3D Printing of Biomedical Materials. *Polym. Chem.* **2016**, *7*, 5169–5180.
- (55) Wallin, T. J.; Pikul, J. H.; Bodkhe, S.; Peele, B. N.; MacMurray, B. C.; Therriault, D.; McEnerney, B. W.; Dillon, R. P.; Giannelis, E. P.; Shepherd, R. F. Click Chemistry Stereolithography for Soft Robots That Self-Heal. *J. Mater. Chem. B* **2017**, *5*, 6249–6255.
- (56) Chen, L.; Wu, Q.; Wei, G.; Liu, R.; Li, Z. Highly Stable Thiol—Ene Systems: From Their Structure—Property Relationship to DLP 3D Printing. *J. Mater. Chem. C* **2018**, *6*, 11561–11568.
- (57) Sycks, D. G.; Wu, T.; Park, H. S.; Gall, K. Tough, Stable Spiroacetal Thiol-Ene Resin for 3D Printing. *J. Appl. Polym. Sci.* **2018**, 135, 46259.
- (58) Childress, K. K.; Alim, M. D.; Hernandez, J. J.; Stansbury, J. W.; Bowman, C. N. Additive Manufacture of Lightly Crosslinked Semicrystalline Thiol–Enes for Enhanced Mechanical Performance. *Polym. Chem.* **2020**, *11*, 39–46.
- (59) Alim, M. D.; Childress, K. K.; Baugh, N. J.; Martinez, A. M.; Davenport, A.; Fairbanks, B. D.; Mcbride, M. K.; Worrell, B. T.; Stansbury, J. W.; Mcleod, R. R.; Bowman, C. N. A Photopolymerizable Thermoplastic with Tunable Mechanical Performance. *Mater. Horiz.* **2020**, *7*, 835–842.
- (60) Esfandiari, P.; Ligon, S. C.; Lagref, J. J.; Frantz, R.; Cherkaoui, Z.; Liska, R. Efficient Stabilization of Thiol-Ene Formulations in Radical Photopolymerization. *J. Polym. Sci., Part A: Polym. Chem.* **2013**, *51*, 4261–4266.
- (61) Li, L.; Chen, X.; Jin, K.; Torkelson, J. M. Vitrimers Designed Both to Strongly Suppress Creep and to Recover Original Cross-Link Density after Reprocessing: Quantitative Theory and Experiments. *Macromolecules* **2018**, *51*, 5537–5546.
- (62) Chen, L.; Zhang, L.; Griffin, P. J.; Rowan, S. J. Impact of Dynamic Bond Concentration on the Viscoelastic and Mechanical Properties of Dynamic Poly(alkylurea-co-urethane) Networks. *Macromol. Chem. Phys.* **2020**, 221, 1900440.
- (63) Ciarella, S.; Sciortino, F.; Ellenbroek, W. G. Dynamics of Vitrimers: Defects as a Highway to Stress Relaxation. *Phys. Rev. Lett.* **2018**, *121*, 058003.